Quantum anomalous Hall insulator phase in asymmetrically functionalized germanene

Chia-Hsiu Hsu, Yimei Fang, Shunqing Wu, Zhi-Quan Huang, Christian P. Crisostomo, Yu-Ming Gu, Zi-Zhong Zhu, Hsin Lin, Arun Bansil, Feng-Chuan Chuang, and Li Huang

Phys. Rev. B **96**, 165426 — Published 16 October 2017

DOI: 10.1103/PhysRevB.96.165426

Quantum Anomalous Hall Insulator Phase in Asymmetrically Functionalized Germanene

Chia-Hsiu Hsu

Department of Physics, Southern University of Science and Technology, Shenzhen, Guangdong 518055, China and

Department of Physics, National Sun Yat-Sen University, Kaohsiung 804, Taiwan

Yimei Fang and Shunqing Wu

Collaborative Innovation Center for Optoelectronic Semiconductors and Efficient Devices and Department of Physics, Xiamen University, Xiamen 361005, China and

Institute of Theory Physics and Astrophysics, Xiamen University, Xiamen 361005, China

Zhi-Quan Huang, Christian P. Crisostomo, and Yu-Ming Gu

Department of Physics, National Sun Yat-Sen University, Kaohsiung 804, Taiwan

Zi-Zhong Zhu

Collaborative Innovation Center for Optoelectronic Semiconductors and Efficient Devices and Department of Physics, Xiamen University, Xiamen 361005, China

Institute of Theory Physics and Astrophysics, Xiamen University, Xiamen 361005, China and

Fujian Provincial Key Laboratory of Theoretical and Computational Chemistry, Xiamen 361005,China

Hsin Lin*

Centre for Advanced 2D Materials and Graphene Research Centre, National University of Singapore, Singapore 117546 and

Department of Physics, National University of Singapore, Singapore 117542

Arun Bansil

Department of Physics, Northeastern University,
Boston, Massachusetts 02115, USA

Feng-Chuan Chuang[†]

Department of Physics, National Sun Yat-Sen University, Kaohsiung 804, Taiwan and
Multidisciplinary and Data Science Research Center,
National Sun Yat-Sen University, Kaohsiung 804, Taiwan

Li Huang[‡]

Department of Physics, Southern University of Science and Technology,
Shenzhen, Guangdong 518055, China

Abstract

Using first-principles computations, we discuss topological properties of germanene in buckled as well as planar honeycombs with asymmetric passivation via hydrogen and nitrogen (GeHN) atoms. GeHN in the planar structure is found to harbor a quantum anomalous Hall (QAH) insulator phase. Our analysis indicates that the buckled GeHN also possesses a QAH phase under tensile strain. We computed the associated Chern numbers and edge states to confirm the presence of the QAH state. In particular, chiral edge bands connecting conduction and valence bands were found at the edges of a planar zigzag GeHN nanoribbon. By considering a range of buckling distances, we demonstrate how the system undergoes the transition from the trivial to the QAH phase between the buckled and planar structures. Finally, we show CdTe(111) to be a suitable substrate for supporting buckled germanene in the QAH phase. Our results suggest that functionalized germanene could provide a robust QAH-based platform for spintronics applications.

Keywords: Quantum anomalous Hall effect, Topological phase transition, Germanene honeycomb, Electronic structure, First-principles calculations.

Introduction

In recent years, topological materials such as two-dimensional (2D) topological insulators (TIs),[1–5], topological crystalline insulators (TCIs)[6–8], and quantum anomalous Hall (QAH)[9,10] insulators have been the focus of wide-ranging studies in search of a new generation of materials for low-power-consuming applications.[1,9–13]. The quantum Hall (QH) effect opened up the possibility of dissipationless spin-transport in a 2D insulator in the presence of a strong magnetic field[14,15]. QAH effect, in contrast, arises through the intrinsic magnetization of the material driven by spin-orbit coupling (SOC) effects, without the need for applying an external magnetic field. [16] QAH effect has been investigated theoretically[17], and realized experimentally in magnetically-doped TI thin films and quantum well systems [18–24] These currently realized QAH materials however are limited to extremely low temperatures. Therefore, there is great need to find new materials in which the QAH phase survives at room temperature. Notably, a viable material in this connection must be a ferromagnetic insulating material with a topologically non-trivial electronic band structure.[3,17,25,26]

A number of 2D materials, mainly in the honeycomb structure with different functionalizations, of elements of groups IV[27,28], V,[29–31] and III-V[32–36] have been predicted to harbor the quantum-spin-Hall (QSH) phase. Recently, bimuthene has been realized on a SiC substrate with a large band gap of 0.8eV,[37] in agreement with our theoretical predictions.[38] However, materials realization of various theory proposals for the QAH phase[24,39–44] remains a continuing experimental challenge. To our knowledge, the possible existence of the QAH phase in the germanene-based films has not been explored in the literature, except in a V-decorated germanene supercell.[45]

With this motivation, here we explore topological properties of germanene honeycombs with chemical functionalization using first-principles calculations with focus on identifying possible new QAH phases.[46] We show that asymmetric functionalization via H and N atoms on opposite sides of the honeycomb can induce ferromagnetism,[43] and generate a number of QAH insulator phases over a reasonable range of lattice constants. We have further confirmed our results by calculating edge states of the corresponding ribbons. Our findings suggest that GeHN films on appropriate substrates (such as CdTe(111)) could provide a new platform for exploiting the QAH effect for energy-efficient spintronics applications.

Methods

Our first-principles calculations were performed within the framework of the density functional theory (DFT) utilizing the generalized gradient approximation (GGA) in the Perdew-Burke-Ernzerhof (PBE) form.[47–51] Projector-augmented-wave (PAW)[52] wave functions with energy cut-off of 500 eV were used in the Vienna Ab-Initio Simulation Package (VASP).[53,54] Atomic positions were optimized for each lattice constant value considered until the residual forces were no greater than 10^{-3} eV/Å. In order to treat the planar case, the Ge atoms were held fixed along the z-direction, while the N and H atoms as well as x-direction and y-direction of Ge atoms were allowed to move to reach the lowest energy configuration. The criteria for convergence for self-consistent electronic structure was set at 10^{-6} eV. A vacuum layer of at least 20 Å along the z direction was used to simulate a thin film. A Γ-centered Monkhorst-Pack[55] grid of 12×12×1 was used for 2D integrations in the Brillouin zone. Berry curvature and edge states were calculated with the Hamiltonian obtained from maximally-localized Wannier functions obtained via the WANNIER90 package.[56] Topological invariants of each structure considered were computed by calculating the Chern number[39,57,58]

$$C = \frac{1}{2\pi} \sum_n \int_{BZ} d^2k \Omega_n, \tag{1}$$

where Ω_n is the Berry curvature of the nth band in the k-space.[58–60]

Results

Figs. 1(a)-(c) illustrate the various 2D crystal structures of germanene honeycombs we investigated where the two sides are decorated with hydrogen and nitrogen atoms (denoted as GeHN throughout this paper). Two different types of honeycombs were considered: planar (PL) and buckled (BK). Total energy as a function of the lattice constant for the PL and BK GeHN film is shown in Fig. 1(d). The computed equilibrium lattice constant is 4.10 and 4.40 Å for the BK and PL film, respectively. A net magnetic moment of 1.2 μB per unit cell is found in both systems. The magnetic moment originates predominantly from the N atom, resembling the behavior of nitrogen adsorption on topological insulator surfaces[46]. By following the evolution of the band structure and the associated Chern number (C) with strain, we could identify different topological phases, which are shown in Fig. 1(d). With

increasing lattice constant, the BK honeycomb is seen to transform from a magnetic metal (3.80−3.96 Å), to a trivial insulator up to 4.35 Å. Subsequently, a semi-metallic QAH phase was identified from 4.36 Å to 4.60 Å , which became an insulating QAH phase with an extremely small gap of a few meV beyond 4.60 Å . On the other hand, the PL GeHN film assumes a QAH insulator phase over lattice constant (a) values from 4.00 to 4.55 Å and becomes a trivial nonmagnetic (NM) insulator above 4.80 Å, passing through a magnetic semimetal phase between 4.55 and 4.80 Å.

Band structure of the planar GeHN film at its equilibrium lattice constant of 4.40 Å is plotted in Fig. 2. Non-spin-polarized results without the SOC in Fig. 2(a) show the presence of two bands touching at the Fermi energy along the high-symmetry line $\Gamma - K$, indicating that GeHN film is a zero-gap material. When spin-polarization is introduced, see Fig. 2(b), a band splitting between the spin-up (red lines) and spin-down (blue lines) channels is observed to develop with both channels exhibiting metallic properties. Inclusion of the SOC (Fig. 2(c)) not only opens a gap in the system but also removes the band degeneracy at the Γ point. Strain dependence of gaps along the $\Gamma - K$ and $\Gamma - K'$ directions is shown in Fig. S1 (Supplementary Materials) in which the asymmetric band structures reflect the breaking of the inversion and time-reversal symmetries[61]. We further examine the PL GeHN film with a larger band gap of 102 meV at 4.08 Å (equilibrium lattice constant of the freestanding germanene film). The non-spin-polarized bands (without the SOC) reveal a semiconducting behavior with a small gap along $\Gamma - K$, see Fig. 2(d). With the inclusion of the spin-polarization (Fig. 2(e)), the gapless spin-up channel and the semiconducting spin-down channel present a system with half-metallic character. A band gap of 102 meV opens up with the SOC, see Fig. 2(f). A number of previous studies of the QAH effect on the honeycomb lattice have reported band inversion only in one spin channel[24,44]. In contrast, our analysis of orbital contributions (Fig. 2(e)) reveals that both the spin-down and spin-up channels undergo band inversions between s and p orbitals at the Γ point. A more detailed analysis (Fig. S2 in Supplementary Materials[61]) demonstrates that the dominant contribution is from the p_z orbitals of N and Ge2 atoms (see Fig. 1(b)), which drives an s-p_z inversion in the spin-down channel. For the spin-up channel, on the other hand, an s-$p_{x,y}$ inversion is involved. These band inversions indicate the appearance of the QAH insulator state, which we have further confirmed via chiral edge state computations discussed below.

We computed Berry curvatures and edge states of the planar GeHN film at the lattice

constant of 4.08 Å in order to assess its topological properties. For this purpose, an effective tight-binding Hamiltonian was obtained as described in the Methods section above. Our tight-binding model well reproduces the first-principles band structure, see Fig. 3(a). Value of the Berry curvature (Fig. 3(b)) is seen to be large around the band inverted region near the Γ point. We obtained a Chern number equal to 1 by integrating the Berry curvature over the first Brillouin zone. Finally, Fig. 3(c) shows the band structure of a planar-zigzag-nanoribbon of GeHN. The size of blue and red circles is proportional to the contributions of the left and right hand side zigzag edges, respectively. For each side of the edge, only one chiral edge state is seen to connect the conduction and valence bands. The number of chiral edge state on each side is equal to the absolute value of the Chern number, confirming the nontrivial band topology.

In order to understand the nature of the topological phase transition as it relates to the buckling of the honeycomb, we now consider the evolution of the band structure as the buckling distance, d_B, increases from 0.2 Å to 0.5 Å at a lattice constant of 4.08 Å , see Figs. 4(a)–(e). Note that the optimization of the structure here was performed with the adjacent Ge atoms kept fixed in terms of the distance d_B in the vacuum direction. By looking at the s-orbital contribution (red circles), we can see a band inversion where the s orbital moves from the valence to the conduction band. The band gap is seen to close at $d_B = 0.37$ Å (Fig. 4(c)), which marks the critical point between the topological and trivial phases. In particular, we can identify a nontrivial phase in Figs. 4(a,b) and a trivial phase in Figs. 4(d,e). These results indicate that a slightly buckled GeHN film also harbors the QAH phase.

In the buckled GeHN film, on the other hand, a QAH effect was also found under tensile strain, while the equilibrium state is a trivial insulator with $a = 4.10$ Å. Note that hydrogen passivation can be used as a simple scheme for modeling effects of substrates and environment on films[38]. As to a suitable substrate, the surface lattice constant of CdTe(111) is 4.68 Å. The spin-polarized band structure of the BK GeHN film at the lattice constant of 4.68 Å is shown in Fig. 5(a). The spin-up and spin-down band structures are seen to cross the Fermi-level around the Γ point with the presence of an SOC-driven gap, see Fig. 5(b). To simulated the substrate-supported GeHN, we resorted the CdTe(111) substrate which had been shown to support honeycomb stanene and harbor the QAH state[24]. Similar to the previous study[24], we considered N atoms adsorbed on one sided of germanene film where the Te-layer of the

CdTe substrate (adjacent to germanene) bond the germanene film on the other side. To test the stability of the CdTe(111) supported GeHN, different configurations were generated by shifting the germanene with respect to the CdTe(111) and by testing N atoms to be adsorbed on different sites. Next, fully structural relaxations were performed for all considered models. We found the lowest-energy model and QAH phase was retained. The atomic structure is shown in Figs. 5(e). The band structures without and with SOC are shown in Figs. 5(c) and (d), respectively. A ferromagnetic ground state with a metallic band structure is seen (without SOC) in Fig. 5(c). Inclusion of the SOC yields a band structure with a gap of 24 meV, which is also well-reproduced by our tight-binding model, see Fig. 5(d). Finally, a chiral edge state connects the valence and conduction bands as shown in Fig. 5(f). The number of chiral edge states correctly equals the absolute value of the Chern number, which in this case is 1.

Conclusions

We have discussed the electronic structures and topological properties of buckled and planar germanene films functionalized asymmetrically with H and N atoms on the two sides (GeHN) using first-principles computations. The GeHN film in the planar honeycomb structure is found to be a QAH insulator over lattice constant (a) values of 4.00−4.55 Å , a trivial nonmagnetic insulator for $a > 4.80$ Å, and a magnetic semimetal over 4.55−4.80 Å. For the buckled case, the QAH phase was found over the lattice constant range of 4.36−4.80 Å. We confirmed the presence of the QAH phase through computations of the Chern number and the edge-state spectrum of a zigzag nanoribbon of GeHN. Slightly buckled structures were also found to support the QAH phase. The GeHN film is shown to undergo a topological phase transition as a function of the size of the buckling distance. Finally, the QAH phase was found to be robust when the buckled germanene film was supported on the CdTe(111) substrate. Our study suggests that asymmetric adsorption on germanene honeycombs could provide a new QAH-effect-based platform for various applications.

Acknowledgements

L. Huang acknowledges the support by the startup of South University of Science and Technology of China, the NSFC under Grant No. 11404160 and Shenzhen Peacock team under Grant No. KQTD2016022619565991. FCC acknowledges support from the National

Center for Theoretical Sciences and the Ministry of Science and Technology of Taiwan under Grants Nos. MOST-104-2112-M-110-002-MY3 and MOST-103-2112-M-110-008-MY3. He is also grateful to the National Center for High-performance Computing for computer time and facilities. SQW and ZZZ also acknowledge support from the National Natural Science Foundation of China under grant No. 11574257. The work at Northeastern University was supported by the US Department of Energy (DOE), Office of Science, Basic Energy Sciences grant number DE-FG02-07ER46352 (core research), and benefited from Northeastern University's Advanced Scientific Computation Center (ASCC), the NERSC supercomputing center through DOE grant number DE-AC02-05CH11231, and support (applications to layered materials) from the DOE EFRC: Center for the Computational Design of Functional Layered Materials (CCDM) under DE-SC0012575. H.L. acknowledges the Singapore National Research Foundation for support under NRF Award No. NRF-NRFF2013-03.

* nilnish@gmail.com

† fchuang@mail.nsysu.edu.tw

‡ huangl@sustc.edu.cn

1. A. Bansil, H. Lin, and T. Das, Rev. Mod. Phys. **88**, 021004 (2016).
2. C. L. Kane and E. J. Mele, Phys. Rev. Lett. **95**, 146802 (2005).
3. X. L. Qi, T. L. Hughes, and S. C. Zhang, Phys. Rev. B **78**, 195424 (2008).
4. M. Z. Hasan and C. L. Kane, Rev. Mod. Phys. **82**, 3045 (2010).
5. X.-L. Qi and S.-C. Zhang, Rev. Mod. Phys. **83**, 1057(54) (2011).
6. L. Fu, Phys. Rev. Lett. **106**, 106802 (2011).
7. T. H. Hsieh, H. Lin, J. Liu, W. Duan, A. Bansil, and L. Fu, Nat. Commun. **3**, 982 (2012).
8. C.-H. Hsu, Z.-Q. Huang, C. P. Crisostomo, L.-Z. Yao, F.-C. Chuang, Y.-T. Liu, B.-K. Wang, C.-H. Hsu, C.-C. Lee, H. Lin, and A. Bansil, Sci. Rep. **6**, 18993 (2016).
9. H. Weng, R. Yu, X. Hu, X. Dai, and Z. Fang, Adv. Phys. **64**, 227–282 (2015).
10. K. He, Physics **8**, 41 (2015).
11. N. Nagaosa, J. Sinova, S. Onoda, A. H. MacDonald and N. P. Ong, Rev. Mod. Phys. **82**, 1539 (2010).

12. X.-L. Qi, Y.-S. Wu, and S.-C. Zhang, Phys. Rev. B **74**, 085308 (2006).
13. K. He, Y. Wang, and Q.-K. Xue, Natl. Sci. Rev. **1**, 38–48 (2014).
14. K. v. Klitzing, G. Dorda, and M. Pepper, Phys. Rev. Lett. **45**, 494 (1980).
15. C. W. J. Beenakker and H. van Houten, Solid State Phys. **44**, 44, 1–228 (1991).
16. F. D. M. Haldane, Phys. Rev. Lett. **61**, 2015 (1988).
17. R. Yu, W. Zhang, H.-J. Zhang, S.-C. Zhang, X. Dai, and Z. Fang, Science **329(5987)**, 61–64 (2010).
18. C.-Z. Chang, J. Zhang, M. Liu, Z. Zhang, X. Feng, K. Li, L.-L. Wang, X. Chen, X. Dai, Z. Fang, X.-L. Qi, S.-C. Zhang, Y. Wang, K. He, X.-C. Ma, and Q.-K. Xue, Adv. Mater. **25**, 1065–1070 (2013).
19. C.-Z. Chang, J. Zhang, X. Feng, J. Shen, Z. Zhang, M. Guo, K. Li, Y. Li, P. Wei, L.-L. Wang, Z.-Q. Ji, Y. Feng, S. Ji, X. Chen, J. Jia, X. Dai, Z. Fang, S.-C. Zhang, K. He, Y. Wang, L. Lu, X.-C. Ma, and Q.-K. Xue, Science **340**, 167–170 (2013).
20. X. Kou, Y. Fan, M. Lang, P. Lang, and K. L. Wang, **215-216**, 34–53 (2015).
21. X. Kou, L. Pan, J. Wang, Y. Fan, E. S. Choi, W.-L. Lee, T. Nie, K. Murata, Q. Shao, S.-C. Zhang, and K. L. Wang, Nat. Commun. **6**, 8474 (2015).
22. C.-Z. Chang, W. Zhao, D. Y. Kim, H. Zhang, B. A. Assaf, D. Heiman, S.-C. Zhang, C. Liu, M. H. W. Chan, and J. S. Moodera, Nat. Mater. **14**, 473–477 (2015).
23. A. J. Bestwick, E.F??J. Fox, X. Kou, L. Pan, and K. L. Wang, Rev. Lett. **114**, 187201 (2015).
24. S.-C. Wu, G. Shan, and B. Yan, Phys. Rev. Lett. **113**, 256401 (2014).
25. S. Oh, Science **340**, 153 (2013).
26. C.-X. Liu, X.-L. Qi, X. Dai, Z. Fang, and S.-C. Zhang, Phys. Rev. Lett. **101**, 146802 (2008).
27. Y. Xu, B. Yan, H.-J. Zhang, J. Wang, G. Xu, P. Tang, W. Duan, and S.-C. Zhang, Phys. Rev. Lett. **111**, 136804 (2013).
28. B.-H. Chou, Z.-Q. Huang, C.-H. Hsu, F.-C. Chuang, Y.-T. Liu, H. Lin, and A. Bansil, New J. Phys. **16**, 115008 (2014).
29. C. C. Liu, S. Guan, Z. Song, S. A. Yang, J. Yang, and Y. Yao, Phys. Rev. B **90**, 085431 (2014).
30. Z. Song, C.-C. Liu, J. Yang, J. Han, M. Ye, B. Fu, Y. Yang, Q. Niu, J. Lu, and Y. Yao, Asia Mat. **6**, e147 (2014).
31. L. Chen, G. Cui, P. Zhang, X. Wang, H. Liu, and D. Wang, Phys. Chem. Chem. Phys. **16**, 17206 (2014).

32. F.-C. Chuang, Z.-Q. Huang, Y.-T. Liu, C.-H. Hsu, T. Das, H. Lin, and A. Bansil, Nano Lett. **14**, 2505–2508 (2014).
33. C. P. Crisostomo, L.-Z. Yao, Z.-Q. Huang, C.-H. Hsu, F.-C. Chuang, H. Lin, M. A. Albao, and A. Bansil, Nano Lett. **15(10)**, 6568-6574 (2015).
34. L.-Z. Yao, C. P. Crisostomo, C.-C. Yeh, S.-M. Lai, Z.-Q. Huang, C.-H. Hsu, F.-C. Chuang, H. Lin, and A. Bansil, Sci. Rep. **5**, 15463 (2015).
35. L. Li, X. Zhang, X. Chen, and M. Zhao, Nano Lett. **15(2)**, 1296 (2015).
36. M. Zhao, X. Chen, L. Li, and X. Zhang, Sci. Rep. **5**, 8441 (2015).
37. F. Reis et al., Science 10.1126/science.aai8142 (2017).
38. C.-H. Hsu, Z.-Q. Huang, F.-C. Chuang, C.-C. Kuo, Y.-T. Liu, H. Lin, and A. Bansil, New J. Phys. **17**, 025005 (2105).
39. Z. Qiao, S. A. Yang, W. Feng, W.-K. Tse, J. Ding, Y. Yao, J. Wang, and Q. Niu, Phys. Rev. B **82**, 161414(R) (2010).
40. J. L. Lado and J. Fernández-Rossier, Phys. Rev. B **92**, 115433 (2015).
41. T. Zhou, J. Zhang, B. Zhao, H. Zhang, and Z. Yang, Nano Lett. **15**, 5149–5155 (2015).
42. C.-C. Liu, J.-J. Zhou, and Y. Yao, Phys. Rev. B **91**, 165430 (2015).
43. K.-J. Jin and S.-H. Jhi, Sci. Rep. **5**, 8426 (2015).
44. S.-P. Chen, Z.-Q. Huang, C. P. Crisostomo, C.-H. Hsu, F.-C. Chuang, H. Lin, and A. Bansil, Sci. Rep. **6**, 31317 (2016).
45. T. P. Kaloni, J. Phys. Chem. C **118**, 25200-25208 (2014).
46. K. H. Jin and S. H. Jhi, J. Phys. Condens. Matt. **24**, 175001 (2012).
47. P. Hohenberg and W. Kohn, Phys. Rev. **136**, B864 (1964).
48. W. Kohn and L. J. Sham, Phys. Rev. **140**, A1133 (1965).
49. D. M. Ceperley and B. J. Alder, Phys. Rev. Lett. **45**, 566 (1980).
50. J. P. Perdew and A. Zunger, Phys. Rev. B **23**, 5048 (1981).
51. J. P. Perdew, K. Burke, and M. Ernzerhof, Phys. Rev. Lett. **77**, 3865 (1996).
52. G. Kresse and D. Joubert, Phys. Rev. B **59**, 1758 (1999).
53. G. Kresse and J. Hafner, Phys. Rev. B **47**, 558 (1993).
54. G. Kresse and J. Furthmüller, Phys. Rev. B **54**, 11169 (1996).
55. H. J. Monkhorst and J. D. Pack, Phys. Rev. B **13**, 5188 (1976).
56. A. A. Mostofi, J. R. Yates, Y.-S. Lee, I. Souza, D. Vanderbilt, and N. Marzari, Comput. Phys.

Commun. **178**, 685–699 (2008).

57. M. Kohmoto, Ann. Phys. N.Y. **160**, 343 (1985).
58. D. J. Thouless, M. Kohmoto, M. P. Nightingale, and M. den Nijs, Phys. Rev. Lett. **49**, 405 (1982).
59. M. C. Chang and Q. Niu, Phys. Rev. B **53**, 7010 (1996).
60. Y. Yao, L. Kleinman, A. H. MacDonald, J. Sinova, T. Jungwirth, D.-S. Wang, E. Wang, and Q. Niu, Phys. Rev. Lett. **92**, 037204 (2004).
61. See Supplemental Material at [URL will be inserted by publisher] for (1) Evolution of band structure under strain; (2) Orbital composition analyses at the lattice constant of 4.08 Å .

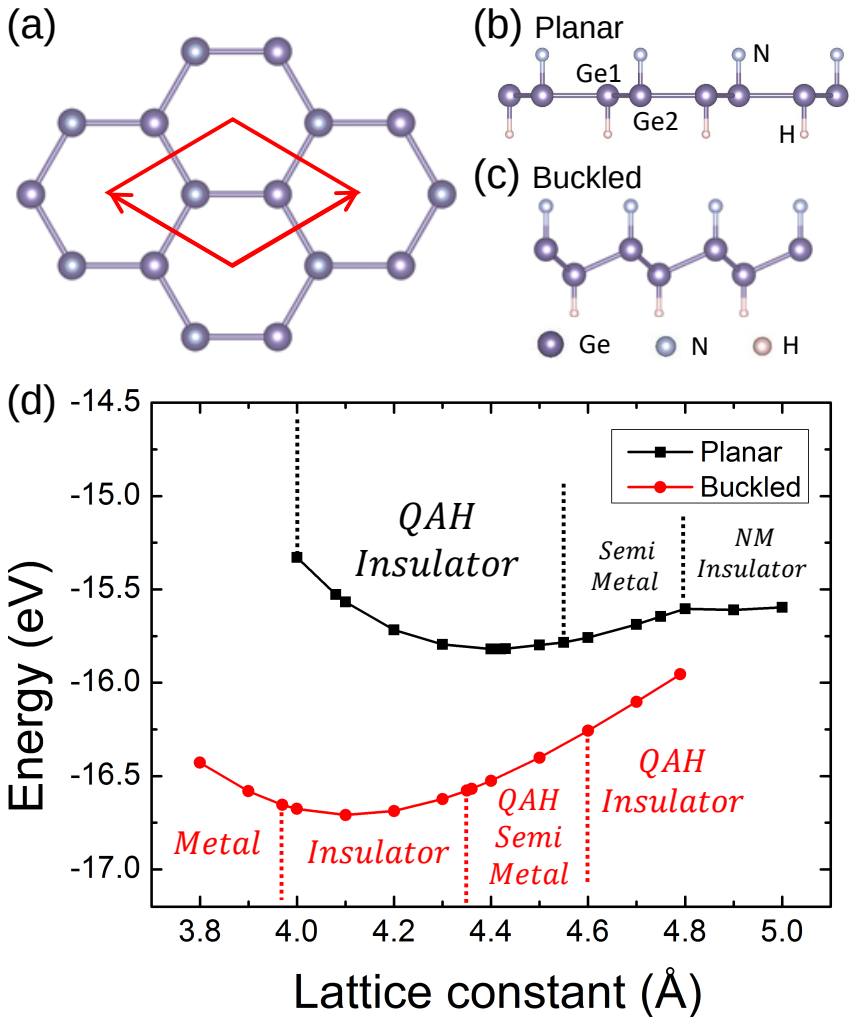

FIG. 1. Crystal structures of germanene honeycombs passivated with hydrogen and nitrogen. (a) Top-view with the primitive cell marked (red line). (b)-(c) Side views of different GeHN films. Hydrogen and nitrogen decoration of germanene with a planar (b) and buckled (c) germanene honeycomb. (d) Total energy per unit cell as a function of the lattice constant. Various phases assumed by the planar (black squares) and buckled (red circles) GeHN films are identified.

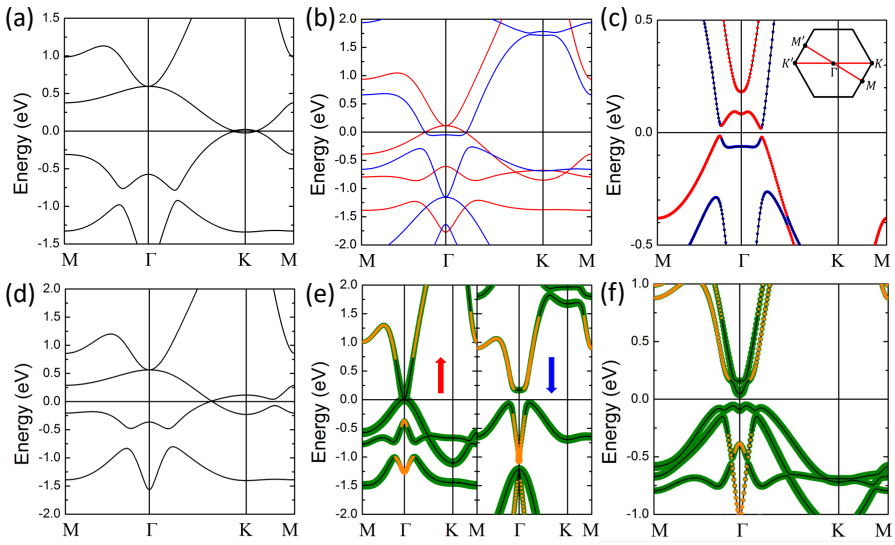

FIG. 2. Band structures of a planar GeHN film at the optimized lattice constant a =4.40 Å. (a) Non-spin-polarized without SOC. (b) Spin-polarized without SOC. (c) Spin-polarized with SOC. Red and blue lines in (b) denote spin-up and spin-down states, and red and blue circles in (c) denote $+mz$ and $-mz$, respectively. Insert in (c) shows the first Brillouin zone in which the high symmetry points are marked. Band structures of a planar GeHN film at a =4.08 Å. (d) Non-spin-polarized without SOC. (e) Spin-polarized without SOC. (f) Spin-polarized with SOC. Filled orange(olive) circles refer to s(p) orbitals where sizes of circles are proportional to the amplitude of the orbital contribution.

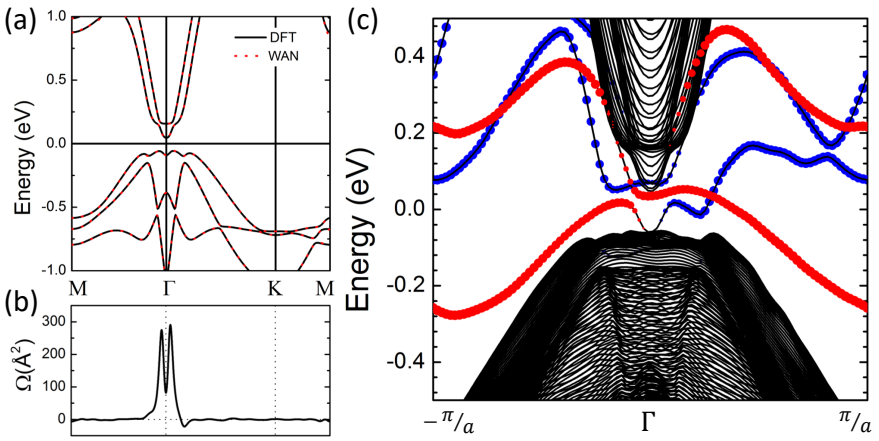

FIG. 3. (a) The first-principles band structure (black lines) is compared with the corresponding results obtained from a Wannier90-based tight-binding fit (red dotted lines) for a =4.08 Å. (b) Berry curvature computed using the tight-binding Hamiltonian. (c) Band structure of a GeHN nanoribbon with zigzag edge. The sizes of blue and red circles are proportional to the contribution from the left- and right-hand-side edges, respectively.

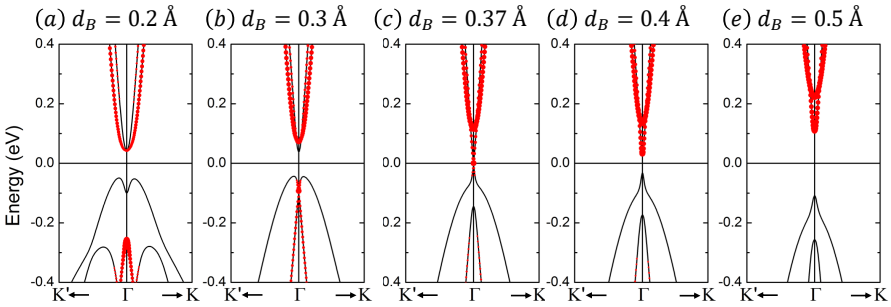

FIG. 4. Topological phase transition in a buckled GeHN film from a QAH insulator to a trivial insulator phase as the buckling distance (d_B) increases at a lattice constant of 4.08 Å . The s-orbital contribution is labeled by red circles.

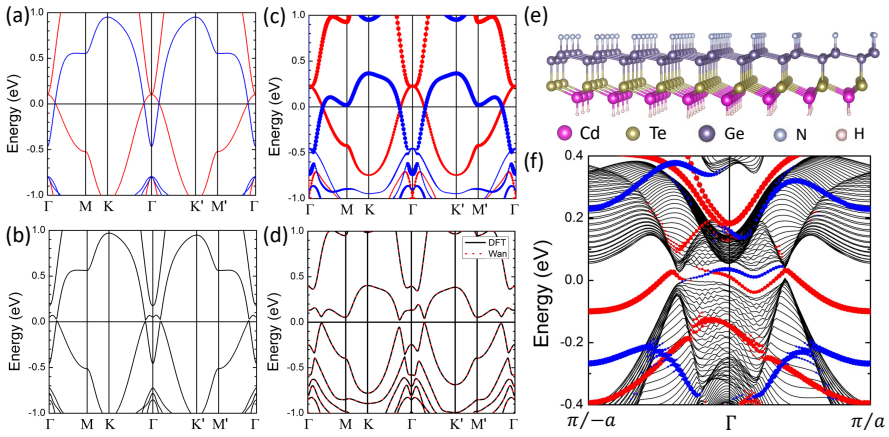

FIG. 5. Band structures of a buckled GeHN film at a =4.68 Å. (a) Spin-polarized without SOC. (b) Spin-polarized with SOC. (c) Spin-polarized band structure of N-adsorbed germanence on Te-terminated surface of CdTe(111) substrate without SOC. The red and blue lines represent the spin-up and spin- down states, and the circles are the contributions from the N and Ge atoms. (d) The first-principles band structure with SOC (black lines) is compared with the corresponding results obtained from a Wannier90-based tight-binding fit (red dotted lines). (e) Crystal structure of N-adsorbed germanence on the Te-terminated surface of CdTe(111) substrate. (f) Band structure of a nanoribbon with zigzag edge. The sizes of blue and red circles in (f) are proportional to the contributions from the left and right hand side edges, respectively.